Resonant and antiresonant bouncing droplets

M. Hubert,[*] D. Robert, H. Caps, S. Dorbolo, and N. Vandewalle

GRASP, Physics Department, University of Liège, B4000 Liège, Belgium

When placed onto a vibrating liquid bath, a droplet may adopt a permanent bouncing behavior, depending on both the forcing frequency and the forcing amplitude. The relationship between the droplet deformations and the bouncing mechanism is studied experimentally and theoretically through an asymmetric and dissipative bouncing spring model. Antiresonance phenomena are evidenced. Experiments and theoretical predictions show that both resonance at specific frequencies and antiresonance at Rayleigh frequencies play crucial roles in the bouncing mechanism. In particular, we show that they could be exploited for bouncing droplet size selection.

I. INTRODUCTION

Bouncing droplets (BDs) on vibrated liquid interfaces attract much attention because of their peculiar properties [1]. Because of the air layer that separates the droplet from the vibrated surface, the droplet is allowed to bounce vertically upon the liquid without coalescing. Nevertheless, the perpetual bouncing behavior is possible under some conditions concerning the acceleration of the surface. This condition reads $\Gamma > \Gamma_{\text{th}}$ where Γ is the ratio between the acceleration of the surface and the acceleration due to gravity, Γ_{th} being a given threshold to reach that may depend on the frequency of oscillation [1,2]. BDs have the great advantage of transporting some quantities of liquid without chemical contamination [3,4]. Moreover, BDs may be either fragmented [5] or used to create controlled microemulsions [6]. It was therefore suggested that those droplets may be used in some microfluidics applications [7]. Depending on the deformability of both droplet and liquid surface, different dynamics are expected as depicted in the work of Terwagne *et al.* [8]. As shown in the latter article, four main regimes are distinguished from each other through the *Ohnesorge numbers* of the droplet and the liquid bath. The definition of the Ohnesorge number reads

$$\text{Oh} = \nu\sqrt{\rho/2a\sigma}, \tag{1}$$

where ν is the kinetic viscosity of the fluid, ρ its density, and a the typical length scale. An Ohnesorge number greater than unity corresponds to a system where damping is more important than capillary effect, and thus the deformability can be neglected between two impacts. Deformability therefore takes place when this number is less than unity. In this article, we will focus on the regime where $\text{Oh}_{\text{Bath}} > 1$ and $\text{Oh}_{\text{Drop}} < 1$. Especially, we will focus on BD deformations and their link with the bouncing dynamics without considering lubrication or wave propagation on the liquid surface. For this purpose, we investigate the BD dynamics experimentally, and we propose a simple model consisting in an asymmetric bouncing spring (ABS). Resonance and antiresonance behaviors are evidenced and rationalized. The latter effect being observed in system made of coupled oscillators [9] and in the case of Fano resonance [10]. From the particular features of both resonance and antiresonance, we propose a way to select

―――――――
[*]Corresponding author: maxime.hubert@ulg.ac.be

bouncing droplet size. Since the concept we provide is general, we expect this model and its subsequent behaviors to be applicable to a broad range of elastic bouncing objects.

II. EXPERIMENTAL SETUP

The experimental setup consists in a container filled with highly viscous silicone oil (Dow Corning 200 Fluid, $\nu = 1000$ cSt) in order to inhibit the surface deformations ($\text{Oh}_{\text{Bath}} \approx 65$). Droplets of viscosity ranging from 5 to 50 cSt are created with a needle. The information relative to the silicon oils for droplets is summed up in Table I. The container is vertically shaken with a pulsation ω and an amplitude A. The maximum acceleration normalized by the gravity, $\Gamma = A\omega^2/g$, is accurately measured with an accelerometer. Figure 1 presents snapshots of a typical bounce for a frequency $f = 50$ Hz. One observes large deformations of the droplet, which experiences periodic changes from oblate to prolate shapes. Moreover, as the droplet detaches from the interface on the crest of each oscillation, some asymmetry in its shape is generated, the top of the droplet being wider than its bottom. This observation is indicated by a white arrow in Fig. 1. The above observations suggest that droplet deformations superimpose with the periodic forcing from the surface, as proposed in earlier works [11,12].

III. RESULTS

Let us consider the plots of Fig. 2. This figure presents the bouncing threshold Γ_{th}, in a logarithmic scale, as a function of the dimensionless forcing frequency Ω_2, as defined later by Eq. (3). By means of this frequency, for each viscosity, droplets of different radii, mass, and density can be compared onto a single curve. For each curve, resonant behavior is observed near $\Omega_2 = 0.5$. For the resonant frequencies of Fig. 2, the droplet bounces onto the surface for $\Gamma_{\text{th}} < 1$; i.e., for a maximal acceleration below g. Indeed, in order to overcome gravity, the droplet stores elastic energy into its deformation and uses this energy for taking off [11]. Although resonance in BD dynamics has already been studied, others features of those curves have not been analyzed. One remarks that, for specific frequencies $\Omega_2 \approx 1.15$, the threshold reaches a maximum. The bouncing threshold in this case can be 20 times higher than the threshold at the resonance. The maxima in the bouncing thresholds

TABLE I. Parameters relative to the silicon oils used in our experiments. The four first rows contain the fluid properties, and the last two rows contain the ξ and μ parameters obtained from experiments and from Eqs. (11) and (12).

Droplet viscosity ν (cSt)	5	20	50
Surface tension σ (N/m)	1.97×10^{-2}	2.06×10^{-2}	2.08×10^{-2}
Density ρ (kg/m^3)	910	949	960
Ohnesorge number Oh$_{Drop}$	0.024	0.096	0.240
Dissipation ξ	0.241	0.253	0.330
Mass distribution μ	0.651	0.701	0.751

correspond to an antiresonance and will be discussed in the following sections.

IV. MODEL

In order to model the curves of Fig. 2, let us focus on the droplet shapes. The natural shape oscillations of a droplet have been described, in the linear regime, by Prosperetti [13] with a series of spherical harmonics, reading

$$R(\theta,\phi) = a + \sum_{\ell=1}^{+\infty} \sum_{m=-\ell+1}^{\ell-1} c_\ell Y_\ell^m(\theta,\phi). \qquad (2)$$

The natural Rayleigh frequency ω_ℓ [14] of each ℓ mode defines a dimensionless frequency Ω_ℓ given by

$$\Omega_\ell = \omega/\omega_\ell = \sqrt{a^3 \rho \omega^2 / \sigma} \sqrt{1/\ell(\ell-1)(\ell+2)}, \qquad (3)$$

The parameter ℓ denotes the characteristic number of the considered spherical harmonic. Please note that because of the radius a in (3), the droplets of different radii can experience different values of Ω_l for a given set of parameters. This observation is the key ingredient of the droplet filter described at the end of this article. By considering that the Y_0^2 axis-symmetric mode dominates others in average during the bouncing dynamics, as observed in our experiments (cf. Fig. 1), one can write the droplet radius as the following decomposition:

$$R(\theta,\phi) \approx a\big[1 + \delta Y_2^0(\theta,\phi)\big], \qquad (4)$$

where δ measures the maximum Y_2^0 deformation. Two pictures of deformed droplets are shown in Figs. 3(a) and 3(b). Those pictures are superposed to theoretical results (grid shapes).
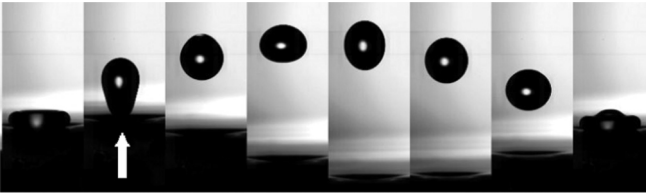

FIG. 1. BD for frequency $f = 50$ Hz, radius $a = 0.76$ mm, and viscosity $\nu = 5$ cSt. One observes that the droplet adopts periodically oblate and prolate shapes. Note that the deformation may be, for instance, asymmetric when the droplet takes off as denoted with a white arrow.
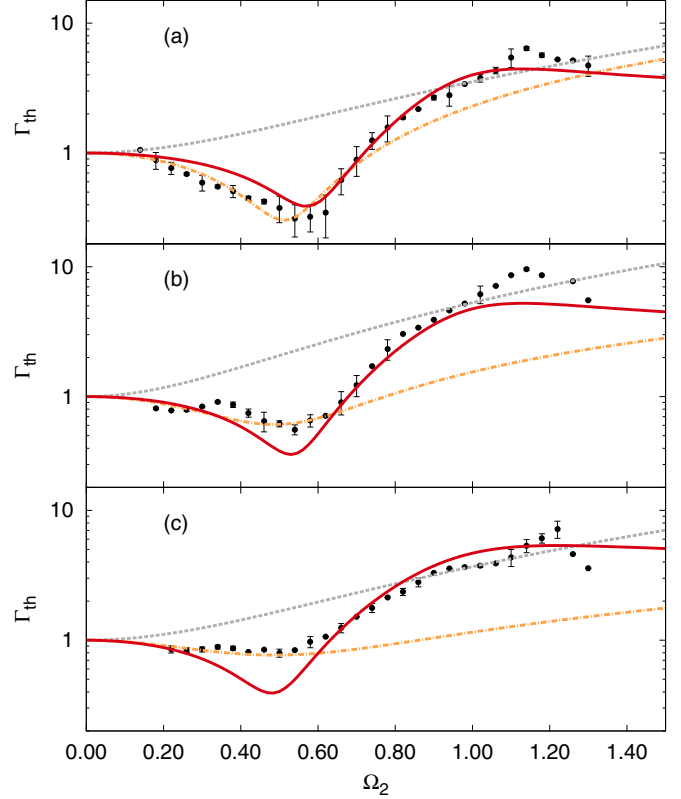

FIG. 2. (Color online) Bouncing threshold (logarithmic scale) as a function of the dimensionless Rayleigh frequency Ω_2 for droplets of different viscosities: (a) 5cSt, (b) 20 cSt, and (c) 50cSt. Black dots represents the experimental data. The curves corresponds to analytical models. Dotted gray line: Couder model [1], dashed orange line: Eichwald model [18], plain red line: our ABS model capturing two extrema while Eichwald captures only resonant behaviors.

They are characterized by oblate ($\delta = -0.318$) and prolate shapes ($\delta = 0.437$).

Computing the surface of the droplet under the appearance of the Y_2^0 spherical harmonic with the constraint of constant volume leads to the plot of Fig. 3(c), showing the evolution of the relative surface energy $\Delta E / E_0$ with respect to δ, E_0 being the surface energy of an undeformed droplet. One observes that $\Delta E / E_0 \propto \delta^2$ in a large interval of δ values. The droplet can therefore be considered as a linear spring while bouncing freely upon the surface. This observation is consistent with previous conclusions made in several articles [11,12,15] and does not contradict the ones obtained by Molacek *et al.* or Chevy *et al.* [16] where some logarithmic spring aims to model the interaction between the droplet and the liquid surface rather than the droplet itself. In conclusion, both descriptions could be seen as complementary.

Based on the above observations, one needs to introduce elasticity, as shown in the previous paragraph, asymmetry, as seen on Fig. 1, and also damping in order to model the BD dynamics. Considering the axis-symmetric Y_0^2 harmonics, we model the droplet as two different masses m_1 and m_2 linked together by a Hookian spring (stiffness k and natural length L) and by a linear damper (dissipation β). The masses m_1 and m_2 can be different in order to account for the asymmetric
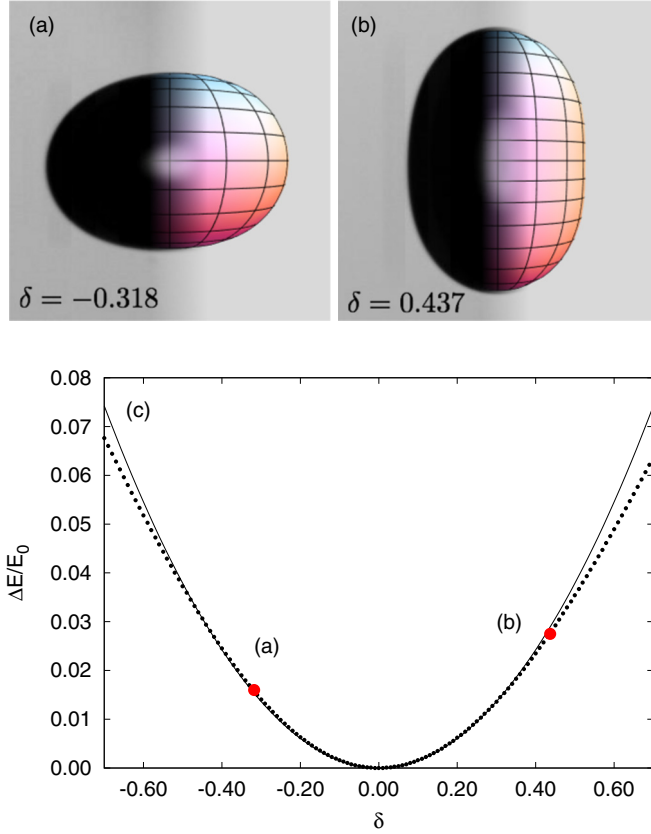
FIG. 3. (Color online) (a) Droplet deformed with $\delta = -0.318$ resulting in an oblate-shaped droplet. The left side is the experimental picture, the right one being the Prosperetti model. (b) Prolate shaped droplet with $\delta = 0.437$. The value of δ in each case has been obtained by fitting the shape of the droplet. (c) Evolution of the relative surface energy for a droplet deformed with the Y_2^0 spherical harmonic, E_0 being the energy of an undeformed droplet (black dots). The plain curve is a guide to the eyes showing the parabolic behavior. The horizontal axis measures the deformation δ. Note also the asymmetric shape of the curve for large δ.

shapes observed during take off in Fig. 1. The spring is used to give some stiffness in order to reproduce resonance and energy storage; more specifically, this stiffness should be linked to the droplet surface tension. The damper captures the dissipation within the droplet when it oscillates. We expect this coefficient to take into account dissipation in the droplet, in the bath and in the air layer. The whole object bounces onto a rigid plate oscillating at the liquid surface amplitude A and angular frequency ω. The plate is chosen to be rigid since the bath beneath the droplet has an Ohnesorge number around 65. Between two successive impacts, the ABS is only submitted to gravity g. Note that this model is unidimensional because of the Y_2^0 axial symmetry. The dynamic of such an object has been described in a previous article [17] in the symmetric case. Defining the mass distribution $\mu = m_1/(m_1 + m_2)$, the spring natural frequency $\omega_0 = \sqrt{k/(m_1 + m_2)}$, the damper dissipation coefficient $\xi = \beta/2\omega_0(m_1 + m_2)$ and $\Omega_0 = \omega/\omega_0$ the dimensionless oscillation frequency, $\Gamma = A\omega^2/g$ the dimensionless surface acceleration, $\phi = \omega t$ the dimensionless time, $l = L/A$ the dimensionless natural length, and $\alpha = z/A$ the

dimensionless height, Newton's second law of motion reads

$$\alpha_p(\phi) = \cos(\phi),$$

$$\ddot{\alpha}_1 + \frac{2\xi\,(\dot{\alpha}_1 - \dot{\alpha}_2)}{\Omega_0\mu} + \frac{(\alpha_1 - \alpha_2 - l)}{\Omega_0^2\mu} + \frac{1}{\Gamma} = 0, \quad (5)$$

$$\ddot{\alpha}_2 - \frac{2\xi\,(\dot{\alpha}_1 - \dot{\alpha}_2)}{\Omega_0(1-\mu)} - \frac{(\alpha_1 - \alpha_2 - l)}{\Omega_0^2(1-\mu)} + \frac{1}{\Gamma} = n_2(\phi).$$

The subscripts p, 1, and 2 are relative to the plate, the upper mass, and the lower mass, respectively. The dot above the symbols denotes the dimensionless time derivative, and n_2 is the dimensionless normal reaction. In the same way than in Ref. [18], the analytic expression of the bouncing threshold can be found and reads

$$\Gamma_{\text{th}}(\Omega_0) = \sqrt{\frac{\left(1 - \mu\Omega_0^2\right)^2 + (2\xi\Omega_0)^2}{\left[1 - (1-\mu)\mu\Omega_0^2\right]^2 + (2\xi\Omega_0)^2}}. \quad (6)$$

Because $\Omega_0 \neq \Omega_2$, the latter frequency describing the free oscillations of the droplet, one has to find the equivalent of this frequency in the ABS case. For this purpose, we consider the equation describing the evolution of $\Delta\alpha = \alpha_1 - \alpha_2 - l$ from the set of Eqs. (5). This yields

$$\ddot{\Delta\alpha} + \frac{2\xi\,\dot{\Delta\alpha}}{\Omega_0\mu(1-\mu)} + \frac{\Delta\alpha}{\Omega_0^2\mu(1-\mu)} = 0. \quad (7)$$

The frequency describing the free oscillation of the ABS, and thus the equivalent of the Rayleigh frequency, is $\Omega_2 = \Omega_0\sqrt{\mu(1-\mu)}$. With this new definition, the ABS bouncing threshold reads

$$\Gamma_{\text{th}}(\Omega_2) = \sqrt{\frac{\left(1 - \frac{\Omega_2^2}{1-\mu}\right)^2 + (2\xi\Omega_2)^2}{\left(1 - \Omega_2^2\right)^2 + (2\xi\Omega_2)^2}}. \quad (8)$$

This bouncing threshold exhibits two extrema in the range $\Omega_2 > 0$, which can be obtained by canceling the derivative of $\Gamma_{\text{th}}(\Omega_2)$ with respect to Ω_2. We obtain

$$\Omega_{\text{Max}} = \sqrt{\frac{\sqrt{\mu^2 + 8(\mu-2)(\mu-1)\xi^2} - \mu + 2}{4(\mu-2)\xi^2 + 2}} \quad (9)$$

$$\Omega_{\text{Min}} = \sqrt{\frac{-\sqrt{\mu^2 + 8(\mu-2)(\mu-1)\xi^2} - \mu + 2}{4(\mu-2)\xi^2 + 2}} \quad (10)$$

Those expressions thus leads to the maximum, i.e., the antiresonance, and minimum, i.e., the resonance, of the bouncing threshold presented in Fig. 2. Knowing the experimental frequencies at which resonance and antiresonance occur, one can inverse the relations (9) and (10) in order to obtain ξ and μ; this will calibrate our ABS model:

$$\mu = \frac{2\Omega_{\text{Max}}^2\Omega_{\text{Min}}^2 - \Omega_{\text{Max}}^2 - \Omega_{\text{Min}}^2}{\Omega_{\text{Max}}^2\Omega_{\text{Min}}^2 - \Omega_{\text{Max}}^2 - \Omega_{\text{Min}}^2}, \quad (11)$$

$$\xi = \frac{\sqrt{\Omega_{\text{Max}}^2 - 1}\sqrt{1 - \Omega_{\text{Min}}^2}}{\sqrt{2\Omega_{\text{Max}}^2 + 2\Omega_{\text{Min}}^2}}. \quad (12)$$

The values of μ and ξ related to the plots of Fig. 2 are given in Table I and correspond to the values used in our

simulations; the corresponding bouncing threshold is shown with plain curves in Fig. 2. In order to compare our ABS model with existing models, we propose in dot-dashed curves the model of Ref. [18] and in the dotted curve the model of Ref. [1]. The first model describes only the deformation of the bath and not those of the droplet, and the second takes into account only the lubrication of the air layer. We observe that the ABS model reproduces both the maximum and the minimum of the bouncing threshold where Couder's model does not show any extrema and Eichwald's model reproduces only the minimum. As a conclusion, one understands that antiresonance in the bouncing droplet dynamics is possible only by considering the deformation of the droplet. Resonance is also captured. Furthermore, one observes that, only knowing the values of Ω_{Max} and Ω_{Min}, the model can be calibrated *a posteriori* and that the results are in a good agreement with experimental data: at low viscosity [Fig. 2(a)], the ABS model coincides correctly with the data. At higher viscosity, the model tends to overestimate the resonant behavior. Indeed, one could discuss the range of validity of the model. Because the model has been developed under the assumption $\text{Oh}_{\text{Drop}} < 1$, the ABS model is not able to capture the dynamics of droplet above this limit. As pointed out in Ref. [2], at high droplet viscosity, the deformation effects are overcome by the air layer dynamics.

Let us focus on the resonant and antiresonant behaviors. Resonance corresponds to large deformation of the droplet. The potential energy stored in this way helps the droplet to take off at low values of Γ_{th}. The dynamics in this case is illustrated on Fig. 4 with spatiotemporal diagrams in the case of a 5cSt droplet. The bottom one corresponds to numerical simulations while the top one corresponds to experimental results. One observes that, despite the simplicity of the model, the calibration of the model made through the knowledge of Ω_{Max} and Ω_{Min} leads to good agreement. Antiresonance appears for $\Omega_2 \simeq 1$, i.e., the resonant frequency of the free droplet. In this case the droplet or ABS oscillates with a phase shift of π with the oscillation of the bath. As a consequence, the elastic properties and the propulsion provided by the bath are always against each other, leading to a high bouncing threshold. Figure 4 also shows the comparison between experimental and numerical spatiotemporal diagrams. Once again, the comparison shows a good agreement between the model and the experiments.

Resonance and antiresonance may find applications in various situations. As an example, we propose to create a droplet-size "filter". For this purpose, one has to observe that the size of a droplet is directly related to its natural Rayleigh frequency [cf. Eq. (3)]. By this means, for a given frequency of oscillation ω, droplets of different sizes can experience different behaviors: resonance (for $\Omega \approx 0.5$) antiresonance (for $\Omega \approx 1$), or anything between. In particular, small droplets would experience resonance, and large droplets would experience antiresonance. The droplet size selector works as follows: The BD is driven at a high-acceleration Γ much higher than the bouncing threshold Γ_{th} for any frequency. When the amplitude of vibration decreases, the acceleration could be lower than the antiresonant droplet condition. In such a situation, all droplets bounce except the ones having a specific size, those experiencing antiresonance.
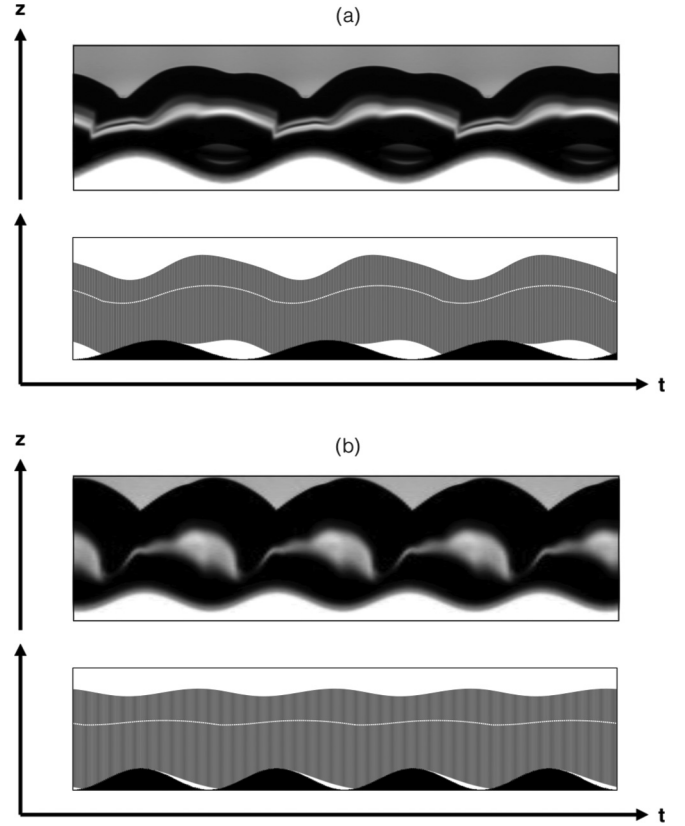

FIG. 4. Numerical and experimental spatiotemporal diagrams for BD with $\nu = 5$ cSt (in arbitrary units). The white region in the experimental diagrams represents the motion of the liquid surface while the black region corresponds to the droplet elongation. The gray curve in numerical simulation is for the elongation of the spring. The white line drawn in the spring motion represents its center of mass. The numerical parameters are those indicated in Table I. (a) Resonant ABS/BD. (b) Antiresonant ABS/BD. One observes in (a) the propulsion of the spring or droplet at the maximum height of the surface motion. (b) The phase opposition of the spring or droplet elongation with the surface oscillation at antiresonance is illustrated.

This corresponds to a band-stop filter. This is shown in the supplementary movie attached to this article [19]. The typical time required for the antiresonant droplet to coalesce is the time required to drain the air layer [20], which is typically 100 bounces. While reducing again the amplitude of vibration, until reaching the lowest value of the threshold, one may only keep the resonant droplets and thus creates a band-pass filter. A specific droplet size is therefore selected. We tested this procedure over a broad range of droplet sizes, and we typically obtained a droplet diameter with a precision of 20 μm. This accurate technique opens new perspectives because it could be exploited for improving experiments [11] for which droplet size is a dominant parameter.

V. CONCLUSION

In this article, we have developed a simple linear model consisting in a asymmetric bouncing spring for droplet bouncing on a liquid surface in the regime $\text{Oh}_{\text{Bath}} > 1$ and $\text{Oh}_{\text{Drop}} < 1$. We have shown that the model gives good quantitative results

through the only knowledge of Ω_{Min} and Ω_{Max}. Indeed, once the model calibrated on the experimental data, it reproduces the droplet bouncing threshold and gives resonant and antiresonant features. Thus, we expect the ABS model to be a useful tool to study a broad case of dynamics. Finally, we showed that resonance and antiresonance could both be used in order to create a droplet size filter which might be of some interest in microfluidic experiments.

[1] Y. Couder, E. Fort, C.-H. Gautier, and A. Boudaoud, Phys. Rev. Lett. **94**, 177801 (2005).

[2] T. Gilet, D. Terwagne, N. Vandewalle, and S. Dorbolo, Phys. Rev. Lett. **100**, 167802 (2008).

[3] A. Eddi, D. Terwagne, E. Fort, and Y. Couder, Europhys. Lett. **82**, 44001 (2008).

[4] S. Gier, S. Dorbolo, D. Terwagne, N. Vandewalle, and C. Wagner, Phys. Rev. E **86**, 066314 (2012).

[5] T. Gilet, N. Vandewalle, and S. Dorbolo, Phys. Rev. E **76**, 035302 (2007).

[6] D. Terwagne, T. Gilet, N. Vandewalle, and S. Dorbolo, Langmuir **26**, 11680 (2010).

[7] N. Vandewalle, D. Terwagne, T. Gilet, H. Caps, and S. Dorbolo, Surf. Coll. A **344**, 42 (2009).

[8] D. Terwagne, F. Ludewig, N. Vandewalle, and S. Dorbolo, Phys. Fluids **25**, 122101 (2013).

[9] S. Belbasi, M. E. Foulaadvand, and Y. S. Joe, Am. J. Phys. **82**, 32 (2014).

[10] U. Fano, Phys. Rev. **124**, 1866 (1961).

[11] S. Dorbolo, D. Terwagne, N. Vandewalle, and T. Gilet, New J. Phys. **10**, 113021 (2008).

[12] A.-L. Biance, F. Chevy, C. Clanet, G. Lagubeau, and D. Quéré, J. Fluid Mech. **554**, 47 (2006).

[13] A. Prosperetti, J. Fluid Mech. **100**, 333 (1980).

[14] Lord Rayleigh, Proc. R. Soc. **29**, 71 (1879).

[15] K. Okumura, F. Chevy, D. Richard, D. Quéré, and C. Clanet, Europhys. Lett. **62**, 237 (2003).

[16] J. Molacek and J. W. M. Bush, J. Fluid Mech. **727**, 582 (2013); Phys. Fluids **24**, 12710 (2012); Chevy *et al.*, Europhys. Lett. **100**, 54002 (2012).

[17] M. Hubert, F. Ludewig, S. Dorbolo, and N. Vandewalle, Physica D **272**, 1 (2014).

[18] B. Eichwald, M. Argentina, X. Noblin, and F. Celestini, Phys. Rev. E **82**, 016203 (2010).

[19] See Supplemental Material at http://link.aps.org/supplemental/10.1103/PhysRevE.91.023017 for this movie.

[20] D. Terwagne, N. Vandewalle, and S. Dorbolo, Phys. Rev. E **76**, 056311 (2007).